

External triggering of plasmoid development at Saturn

A. Kidder,¹ C. S. Paty,² R. M. Winglee,¹ and E. M. Harnett¹

Received 15 February 2012; revised 9 May 2012; accepted 22 May 2012; published 7 July 2012.

[1] The Cassini spacecraft has encountered multiple plasmoids in Saturn's magnetotail thought to be produced by tail reconnection. However, single spacecraft measurements make it difficult to determine plasmoid size, where they form, the composition, and the geometry of the plasma sheet when plasmoids are produced. This paper examines these issues using 3D multifluid simulations of the Kronian magnetosphere. Plasmoids may develop in multiple sectors, form at different distances from the planet, and grow to sizes large relative to the system ($\sim 25 R_S$), with varying widths and lengths. These plasmoids are composed primarily of water group ions and move downtail with speeds of ~ 250 km/s (the local Alfvén speed). The plasma sheet is hinged upward both prior to and following plasmoid formation. Plasmoids can be externally triggered by both flips in the orientation of the interplanetary magnetic field (IMF) as well as a pulse in the solar wind dynamic pressure.

Citation: Kidder, A., C. S. Paty, R. M. Winglee, and E. M. Harnett (2012), External triggering of plasmoid development at Saturn, *J. Geophys. Res.*, 117, A07206, doi:10.1029/2012JA017625.

1. Introduction

[2] In its multiyear mission, the Cassini spacecraft has toured Saturn's inner and outer magnetosphere and made flybys of multiple moons. During the primary mission, Cassini was located primarily in the equatorial plane with trajectories covering the dawn sector. The magnetotail current sheet was observed to be displaced northward from the magnetic equator. Given that these measurements were taken at all local times, the current sheet is warped upward into a bowl-like shape [Arridge *et al.*, 2008]. This upward hinging of the plasma sheet is unlike that found in the terrestrial or Jovian magnetospheres. The terrestrial current sheet is known, however, to support flapping motions, and the Cluster spacecraft observes vertical oscillations with speeds >100 km/s with an amplitude of $\sim 1 R_E$ with a period of ~ 3 min [Sergeev *et al.*, 2003]. A dynamic and flapping Kronian current sheet has also been detected by Cassini when the sheet passes over the spacecraft in the equatorial plane [Arridge *et al.*, 2008]. As Saturn's magnetosphere has a bowl shape, the location where the bending upward begins to occur is known as the hinging location. In addition to hinging upward in the outer magnetosphere, Saturn's magnetosphere is hinged on the dayside as well. This dayside current sheet extends to the magnetopause and shows asymmetries in terms of thicknesses. While the nightside plasma sheet is

confined to a total thickness of about $10 R_S$ and is tilted at an angle of 10° relative to the equatorial plane, the dayside plasma sheet is much broader. The plasma sheet geometry leaves a broad region from $\pm 50^\circ$ latitude [Sergis *et al.*, 2009]. Additionally, heavier O^+ populations are often the dominant component in the energetic particle pressure (compared to H^+) in the dayside plasma sheet [Sergis *et al.*, 2009].

[3] The morphology of this warped current sheet at Saturn also affects the frequency with which Cassini (in the equatorial plane) observes plasmoids traveling downtail. A plasmoid alters the flapping and geometry of the plasma sheet as it moves, and in some instances enabled the spacecraft to encounter a plasmoid directly, or to encounter an indicator of a plasmoid in the form of a traveling compression region (TCR) [Jackman *et al.*, 2007]. As oppositely directed magnetic fields reconnect across the current sheet in the tail (pinching it off), plasma escapes and the tail dipolarizes. Jackman *et al.* [2007] performed a systematic study of Cassini magnetometer (MAG) and plasma spectrometer (CAPS) data to search for magnetic and plasma signatures of spacecraft encounters with plasmoids, discovering three plasmoid events indicative of production by tail reconnection. All three were near midnight or the post-midnight sector, and between 40 and $50 R_S$ downtail. Hill *et al.* [2008] provided density and ENA measurements for these same events, and calculated a reconnection site of $\sim 26.5 R_S$. Two further plasmoid events were described by Jackman *et al.* [2008] at different distances ($\sim 28 R_S$ and $\sim 62 R_S$) but again both in the post-midnight sector ~ 1.5 SLT (Saturn Local Time). The composition and downtail positions again depend upon whether the plasmoid passed over the Cassini spacecraft close after its formation or in the form of a TCR as the plasma expands as it moves downtail. Hill *et al.* [2008] saw water group ion plasma, indicative of the plasmoid's formation in the inner magnetosphere.

[4] Recently, 34 plasmoid observations have been added [Jackman *et al.*, 2011] and have been observed to occur as

¹Department of Earth and Space Sciences, University of Washington, Seattle, Washington, USA.

²School of Earth and Space Sciences, Georgia Institute of Technology, Atlanta, Georgia, USA.

Corresponding author: A. Kidder, Department of Earth and Space Sciences, University of Washington, Box 351310, Seattle, WA 98195-1310, USA. (ariah@uw.edu)

©2012. American Geophysical Union. All Rights Reserved.
10.1029/2012JA017625

single encounters but also in short bursts of two or more. For the five observed plasmoid events of the main mission, Cassini was fortuitously positioned near midnight SLT and around 50 R_S downtail, in order to encounter the flapping current sheet. In searching the MAG data set, *Jackman et al.* [2007] searched the pre-midnight and pre-dawns sectors in a range from ~ 25 to past 75 R_S downtail. The dusk to midnight sector was not visited by Cassini, so there is little information on plasmoid formation, or lack of it, in this sector. In determining which magnetic signatures qualified as a plasmoid, it was required that the field lines moved from a tail-like to a dipole-like configuration, as indicated by a turning of the B_θ component of the magnetic field across the tail current sheet. If the spacecraft is past/planetward of the reconnection point this manifests as a northward/southward turning of the B_θ component. The plasmoid ions must be significantly energized and the plasma flow significantly moved tailward, and not in corotation. Small periodic changes in the north-south component of the magnetic field, in combination with periodic density enhancements are not plasmoids, however, and are associated with plasma sheet flapping [*Jackman et al.*, 2009]. For the five plasmoid events that had this northward turning magnetic signature, speeds have been estimated based on the limited data. The event on March 4, 2006 was ~ 1.1 – $1.4 R_S$ /min, suggesting a speed of 500 km/s [*Hill et al.*, 2008]. Strong dipolarization was observed between 40 and 50 R_S and calculations led to an estimate of the occurrence (based on addition and removal of flux from the system) of between 3 and 5 Saturn ‘substorms’ every ~ 25.5 day solar rotation. In looking at the limited electron and ion data available, the CAPS ELS signatures show an enhancement in electron flux, followed by an abrupt cut off of the high energy population, indicating a sudden evacuation of plasma from the plasma sheet [*Jackman et al.*, 2008]. Limited ion composition data showed that the plasmoid composition was largely dominated by water group ions [*Hill et al.*, 2008], suggesting that it originated in the inner magnetosphere.

[5] Unfavorable observing geometry and lack of orbit time near the tail current sheet is responsible for Cassini’s inability to estimate occurrence frequency of plasmoids, as well as shape, velocity and approximate size. Definitive statements about preference for formation in or travel toward particular sectors are also impossible until Cassini has visited all of these sectors. Since this handful of Cassini observations of the growth and development of plasmoids in Saturn’s magnetotail provides only part of the story, this paper makes use of 3D multifluid modeling with the aim of determining plasmoid size (including three dimensional shape during plasmoid evolution), as well as composition, speed and location. This paper is organized as follows: section 2 will detail the multifluid model and conditions used; model results in section 3 will explain how the geometry of the plasma sheet changes when plasmoids are produced, the composition and characteristics of plasmoids (including size, shape, speed and location), and the upstream conditions that cause plasma sheet warping and plasmoid formation. A summary of the results is given in section 4.

2. Multifluid Model

[6] MHD and multifluid models have been developed to study Saturn’s global plasma interaction, while hybrid

models have been used to examine Titan’s induced magnetosphere. 2D models have recently probed the neutral and plasma interaction in Saturn’s inner magnetosphere.

[7] Global MHD simulations have been used to investigate the overall shape of Saturn’s magnetosphere, including the formation of vortices during various IMF conditions [*Fukazawa et al.*, 2007]. Another MHD study has determined how the position of the bow shock and magnetopause as a function of solar wind conditions [*Hansen et al.*, 2005]. MHD simulations have also examined the tail reconnection as a function of solar wind dynamic pressure [*Zieger et al.*, 2010]. They found that plasma is lost continuously in the magnetotail for cases of high solar wind dynamic pressure and periodic reconnection occurs for medium dynamic pressure. Other factors affect the periodicity as well, including the axial tilt and increased mass loading.

[8] Multifluid modeling has examined the development of the centrifugal interchange instability in Saturn’s inner magnetosphere [*Kidder et al.*, 2009]. Enhanced convection of plasma from Enceladus (as a result of increased convective electric field from anti-parallel IMF or increased outflow from an Enceladus plume) leads to an interchange instability. Cool heavy ions from the Enceladus torus move outward and hotter tenuous plasma moves inward, leading to the formation of interchange fingers. *Kidder et al.* [2009] showed that interchange finger development can be enhanced by certain internal and external conditions. Increased convection when the IMF is anti-parallel to Saturn’s magnetic field allows for growth in the inner magnetospheric plasma that is centrifugally interchanging. In addition, increased plasma densities in the Enceladus ion torus produce an enhancement in plasma interchange. The Rice Convection Model has also been used to simulate the centrifugal interchange instability [*Liu et al.*, 2010] for the region $2 R_S < L < 12 R_S$. Using an active distributed Enceladus source, they show that the Coriolis force inhibits finger growth and that the radial speeds of the inflowing channels are much faster than the speeds of the outflowing channels.

[9] *Brandt et al.* [2010] simulated ENA images of the particle distributions to compare to hydrogen images from the INCA instrument onboard Cassini. They detail how particle distributions that are injected and then drift around Saturn cause the periodicity observed in the magnetic field data from Cassini.

[10] If we are to model the growth and development of plasmoids as they travel downtail it is necessary to model the plasma sheet and plasma flow on a global scale while retaining the dynamics of different mass ions. In order to model the multiple ion populations of the inner magnetosphere, we look past MHD, which is a single-fluid model, and include multiple ion populations with individual temperatures and velocities for each species. Many of the important questions that Cassini is hoping to answer require the ability to resolve the acceleration and energization of the different ion species. Other unresolved issues central to the Cassini campaign require the ability to examine these interactions on a large scale, in order to describe the current sheet morphology and the development of plasmoids at Saturn.

[11] The multifluid treatment is a global model using three ion fluids and an electron fluid. Cassini has observed hot, tenuous plasma interchanging with cool, denser plasma in the centrifugal interchange cycle. Simulations by *Kidder et al.*

[2009] demonstrated that interchange finger development can be enhanced by certain internal and external conditions. Increased convection when the IMF is anti-parallel to Saturn's magnetic field enhances the growth rate of the interchange instability in the inner magnetosphere. In addition, increased plasma densities in the Enceladus ion torus adds to the growth of interchange instability.

[12] A local Titan model [Snowden *et al.*, 2007] has been successfully embedded in the framework of the global Saturn model, coupling the two into a multifluid/multiscale Saturn-Titan model. Winglee *et al.* [2009] used this model to demonstrate how solar wind, IMF and the plasma disk affect Titan, when it is located in the pre-midnight sector. Snowden *et al.* [2011a, 2011b] have used this model to detail Titan's interaction with Saturn's magnetopause at the pre- and post-noon sectors. The multifluid model is described in more detail for the terrestrial case [Winglee, 2004] and has been used to model the terrestrial post plasmoid current sheet at high resolution [Harnett *et al.*, 2006] as well as detailing the relative timing of substorm processes [Winglee *et al.*, 2009].

2.1. Multifluid Treatment

[13] The multifluid equations (1)–(3) track the different ion species as individual fluids through separate equations for mass, momentum and pressure. The subscript α denotes an individual ion or electron population.

$$\frac{\partial \rho}{\partial t} + \nabla \cdot (\rho \mathbf{v}_\alpha) = 0 \quad (1)$$

$$\rho_\alpha \frac{d\mathbf{v}_\alpha}{dt} = n_\alpha q_\alpha (\mathbf{E} + \mathbf{v}_\alpha \times \mathbf{B}) - \nabla P_\alpha - \left(\frac{GM_S}{R^2} \right) \rho_\alpha \hat{\mathbf{r}} \quad (2)$$

$$\frac{\partial P_\alpha}{\partial t} = -\gamma \nabla \cdot (P_\alpha \mathbf{v}_\alpha) + (\gamma - 1) \mathbf{v}_\alpha \cdot \nabla P_\alpha \quad (3)$$

where ρ_α is the mass density, \mathbf{v}_α the bulk velocity, n_α the number density and q_α the charge. G is the gravitational constant, M_S the mass of Saturn, \mathbf{E} the electric field, \mathbf{B} the magnetic field. P_α is the pressure for each ion species and γ is the ratio of specific heats (5/3).

[14] The electron dynamics are described with a pressure equation where the electron velocity is assumed to be determined by drift motion, \mathbf{v}_{de} (i.e., $\frac{d\mathbf{v}_e}{dt} = 0$ in (2)).

$$\frac{\partial P_e}{\partial t} = -\gamma \nabla \cdot (P_e \mathbf{v}_{de}) + (\gamma - 1) \mathbf{v}_{de} \cdot \nabla P_e \quad (4)$$

Approaching this limit, the modified Ohm's law becomes:

$$\mathbf{E} = - \sum_i \frac{n_i}{n_e} \mathbf{v}_i \times \mathbf{B} + \frac{\mathbf{J} \times \mathbf{B}}{en_e} - \frac{\nabla P_e}{en_e} + \eta(\mathbf{r}) \mathbf{J} \quad (5)$$

where n_e is the electron number density, e the electron charge, \mathbf{J} the current density and η the resistivity, added to allow finite conductivity only in Saturn's ionosphere. Everywhere else the conductivity is zero, so there is no anomalous resistivity in our model to drive reconnection.

[15] Modeling the ion and electron components separately allows us to retain the Hall and pressure gradient terms in

Ohm's law (5), which are sufficient to drive reconnection. On substituting (5) into the momentum equation we obtain:

$$\rho_\alpha \frac{d\mathbf{v}_\alpha}{dt} = \frac{q_\alpha n_\alpha}{en_e} (\mathbf{J} \times \mathbf{B} - \nabla P_e) - \nabla P_\alpha + q_\alpha n_\alpha \left(\mathbf{v}_\alpha - \sum_i \frac{n_i}{n_e} \mathbf{v}_i \right) \times \mathbf{B} + q_\alpha n_\alpha \eta \mathbf{J} - \frac{GM_S}{R^2} \rho_\alpha \hat{\mathbf{r}} \quad (6)$$

If one assumes a single ion species or a single velocity for all the species, then (5) reduces to the ideal MHD equation. For different ion species with different velocities, however, the middle term in (6) (i.e. $q_\alpha n_\alpha (\mathbf{v}_\alpha - \sum_i \frac{n_i}{n_e} \mathbf{v}_i) \times \mathbf{B}$), neglected in MHD, is in fact nonzero and will contribute to the development of ion cyclotron effects.

2.2. Grid System

[16] The equations for the multifluid treatment are solved using a 2nd order Runge-Kutta method on a nested grid. The nested grid has highest resolution centered around the planet, with the spherical inner boundary at 2.25 R_S . The coordinate system is such that x is in Saturn's equatorial plane and a positive value points away from the Sun. The positive z -direction points along the magnetic north pole, and the y coordinate completes the system. The z -direction is also aligned with Saturn's rotation axis. The inner magnetosphere resides in the inner-most grid of the simulation, which extends $\pm 15 R_S$ in the x - and y -directions and $\pm 7.5 R_S$ in the z -direction, and is resolved to 1/4 R_S . The outer magnetosphere is covered over a range of 480 R_S , 76 R_S sunward and 404 R_S downtail in the x -direction, ± 240 in the y -direction and ± 120 in the z -direction. The resolution in the nested grid decreases by a factor of two from the highest resolution (inner-most) box to the lowest resolution (outer-most) box.

2.3. Initial Conditions

[17] In the simulation, the solar wind is blown in from the negative x -direction with a velocity of ~ 400 km/s and is angled 28° upward, to account for Saturn's tilt relative to its orbital plane during southern hemisphere summer. The solar wind has been assigned a density of 0.05 protons cm^{-3} , a temperature of 1.4 eV and an IMF of magnitude ± 0.4 nT in \hat{z} . The model is first run for 30 h at zero IMF to establish an appropriate equilibrium for the magnetosphere. IMF is then propagated in for 18 more hours, long enough to remove any initialization effects, before the times for the results shown in this paper.

[18] The three ion components are H^+ , assumed to be from the solar wind or Saturn's ionosphere, a medium mass water group ion, W^+ , of mass 16 amu, and a 32 amu heavy mass species such as O_2^+ . The Enceladus ion source is incorporated in the model by placing an ion torus of W^+ with a density of 2 cm^{-3} at Enceladus' orbit, consistent with observations [Young *et al.*, 2005]. The plasma torus is initialized on field lines that enclose Enceladus' L-shell at 4 ± 0.5 . This yields an extended torus that would be associated with ionization of neutrals well away from Enceladus. Heavy ions are also initialized in this region as a tracer ion species with a density of 0.25 cm^{-3} [Young *et al.*, 2005]. A predominantly H^+ ionosphere is assumed at the inner boundary of 2.25 R_S , representing Saturn's ionosphere. This density is held

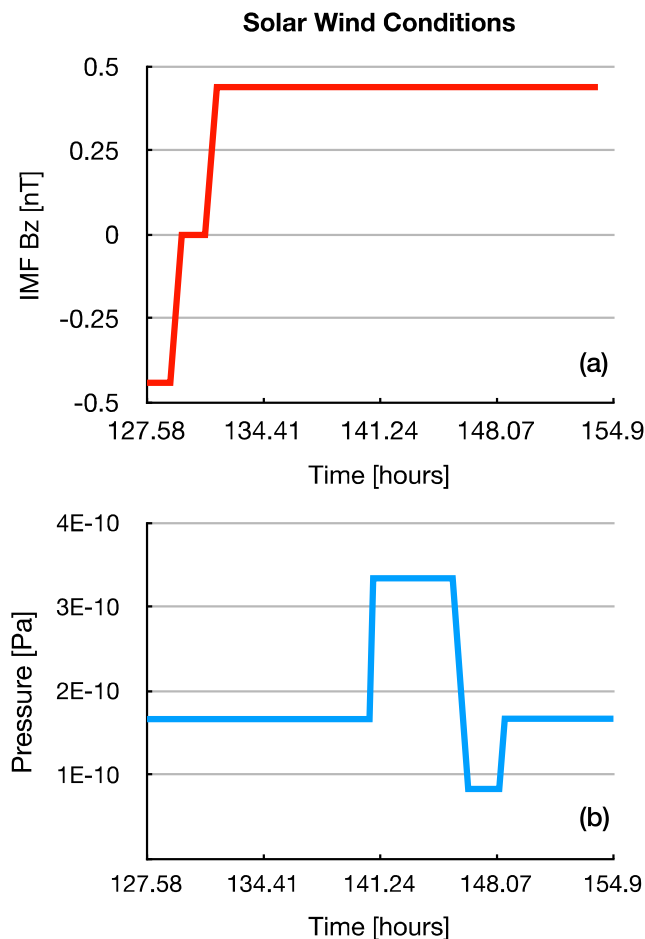


Figure 1. Upstream solar wind conditions (a) a flip in the IMF from -0.4 nT (parallel to Saturn’s planetary field) to $+0.4$ nT (anti-parallel) followed by (b) a doubling of the solar wind dynamic pressure.

constant at a value of 50 cm^{-3} . The ionospheric temperature gradient ranges from 18 eV at the equator to 1 eV at the poles. The temperature is also held constant at the inner boundary. Each species evolves with different temperatures and velocities away from the inner boundary as determined by the formulas in the previous section. The inner boundary assumes a plasma with prescribed density and temperature but no bulk velocity, which leads to a small thermal, or polar, wind. Enhanced outflow is produced as a result of the convection of magnetic field through the system. Saturn is assumed to have a dipolar magnetic field with the opposite polarity of Earth, and equatorial field strength equal to 21,000 nT. We examine the morphology of the plasma sheet and the development of plasmoids in the tail for anti-parallel IMF at ± 0.4 nT and pulse doubling the solar wind dynamic pressure from 1.67×10^{-10} to 3.34×10^{-10} nPa. The Saturn multifluid model does not include the effects of dust or neutral particles, which can significantly affect magnetospheric dynamics. The incorporation of charge exchange in self-consistent ion and neutral fluids has been included in a local multifluid model around Enceladus [Paty *et al.*, 2011]. Future work to include such interactions between ion and neutral fluids in a global Saturn or coupled Saturn-Enceladus model may be useful.

[19] Cassini MAG data has yielded definitive signatures of plasmoids in the regions it has traversed in Saturn’s magnetotail. The five plasmoids detailed by Jackman *et al.* [2008] come from orbits in 2006 covering the post-midnight sector of the equatorial plane in a range from ~ 30 – $60 R_S$ downtail. Jackman *et al.* [2008] believe that these plasmoids preferentially form in the post-midnight sector. This is not a definitive statement, however, since Cassini does not have coverage in the dusk to midnight quadrant. Other difficulties include the fact that a plasmoid may develop in a plane above Cassini, as well as the fact that only a part of a plasmoid may sweep past the spacecraft. Reconnection may appear to be preferentially occurring in the post-midnight sector because rotation will sweep any formed in the dusk sector this direction.

[20] Unfortunately, there is no upstream solar wind monitor at Saturn which would enable Cassini to determine what conditions form plasmoids better than others. In January of 2004 when Cassini was still on its way to Saturn, a joint campaign was conducted with HST to capture auroral images and compare them to the solar wind Cassini was sampling. Crary *et al.* [2005] indicate that solar wind dynamic pressure has the greatest effect on the auroral activity at Saturn. As a result and detailed below, in our model we tried varying two upstream conditions: the orientation of the IMF, and varying the solar wind pressure. Plasmoids in Saturn’s magnetosphere are clearly three-dimensional structures that are easily missed if one simply looks in the equatorial plane, and as a result modeling is necessary to gain a three-dimensional perspective. As we will see, there are external triggers for plasmoid formation, but the question of internal triggers for plasmoid formation at Saturn has yet to be answered.

[21] In the multifluid model we use the term flux ropes for small scale events and the term plasmoid for large scale events. Flux ropes, which we define as small scale ($< 10 R_S$), form at the magnetopause as well as along the flanks during transition times between parallel and anti-parallel IMF. These are different from plasmoids primarily in their size and do not represent a large-scale pinching off of Saturn’s tail. It was important to establish a method to distinguish plasmoids from flux ropes at Saturn, so we determined that a flux rope at Saturn may be large (i.e., larger than a plasmoid at Earth), whereas a plasmoid at Saturn had to be large relative to the system, $> 25 R_S$.

[22] The conditions upstream of Saturn, which provide the external triggers for plasmoid production, are shown in Figure 1. Figure 1a shows a flip in the IMF from parallel to anti-parallel, which produces a plasmoid that is rather large in the y -direction and extends across both the pre- and post-midnight sectors. Figure 1b shows the pulse in solar wind dynamic pressure, which produces a plasmoid in the pre-midnight sector. This increase in solar wind pressure was a result of increasing the velocity by 40%. Solar wind dynamic pressure is expected to increase for example started by the forward shocks of the compression regions of corotating interaction regions [Jackman *et al.*, 2004].

3. Results

3.1. Triggering by a Flip in the Orientation of the IMF

[23] Figure 2 demonstrates the complete process over the span of nearly 20 h, or about 2 rotations of the planet, during

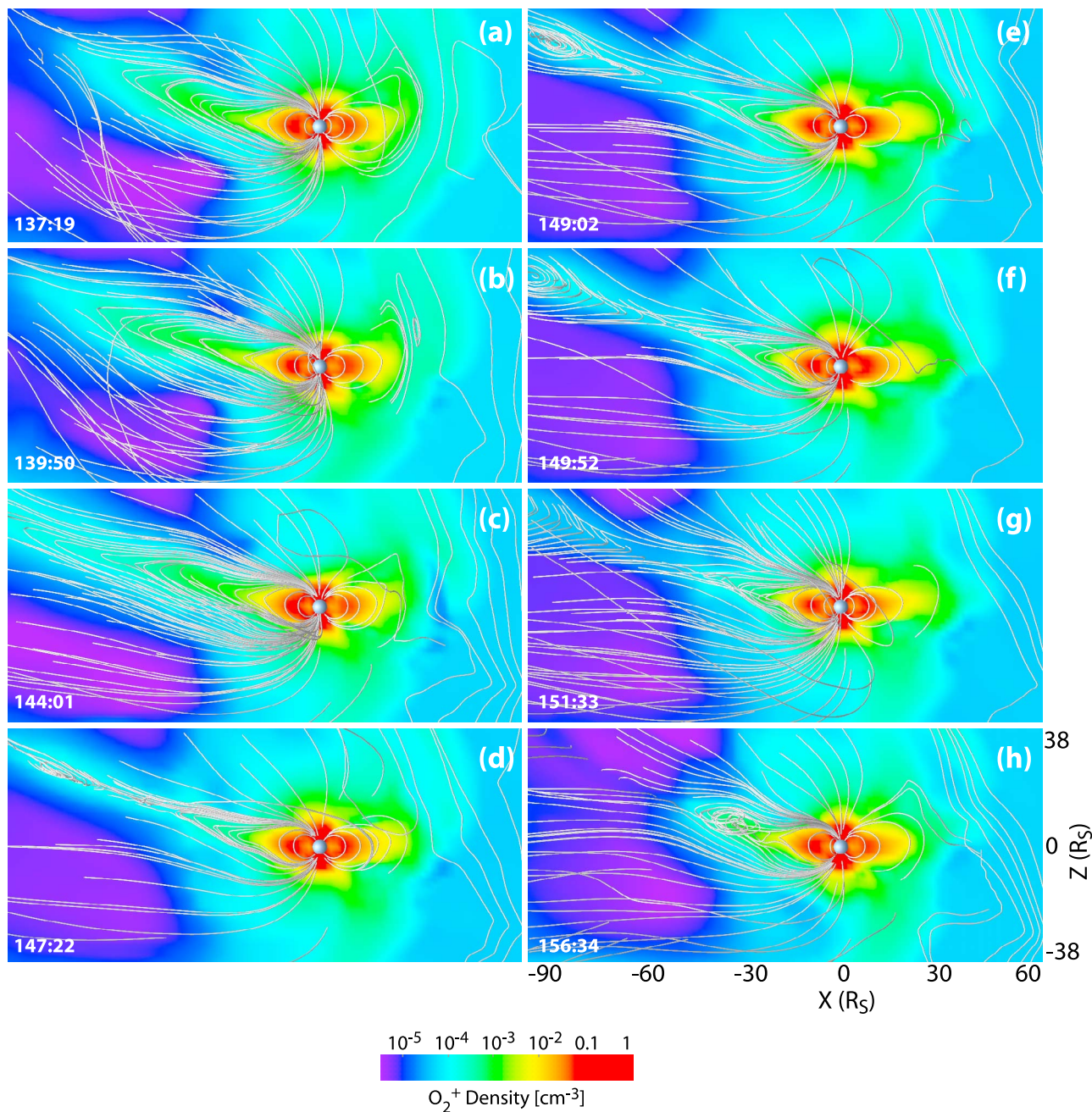


Figure 2. Dawn-side view of O_2^+ density in the noon-midnight meridian. White lines are magnetic field lines. Development of two plasmoids over ~ 20 h shows the plasma sheet thinning and the plasmoid moving downtail as well as up out of the equatorial plane.

which time the solar wind conditions go from a flip from parallel $[0,0,-0.4]$ nT to anti-parallel IMF B_z $[0,0,0.4]$ nT followed by a doubling of the solar wind dynamic pressure. The plasma sheet is hinged upward at $\sim 20 R_S$ with stretched field lines (Figure 2a) and is elongated at this angle for a little over an hour before it thins (Figure 2d) and reconnection occurs at a far neutral line around $60 R_S$. The plasma sheet then thickens and ion density increases before a plasmoid is formed as reconnection occurs at a near neutral line around $30 R_S$ (Figures 2e and 2f). During this evolution the plasma sheet remains bent upward at an angle of 10° . After the

plasmoid moves downtail, the plasma sheet remains broken off at the hinge point as the magnetic field lines dipolarize.

[24] Figure 3 shows the development of a plasmoid shown in Figure 2 in terms of its effect on O_2^+ density. Loading of inner magnetospheric plasma is seen at the early times (138.2 h–139.0 h). A subcorotational cold, heavy interchange finger can be seen in the dusk sector in the equatorial plane at 139.0 h. Thinning of the plasma sheet is seen between 146.5 h and 148.2 h, followed by reconnection up out of the plane at 150.7 h. An x-line develops and heavy plasma continues to move downtail and up from the equatorial plane.

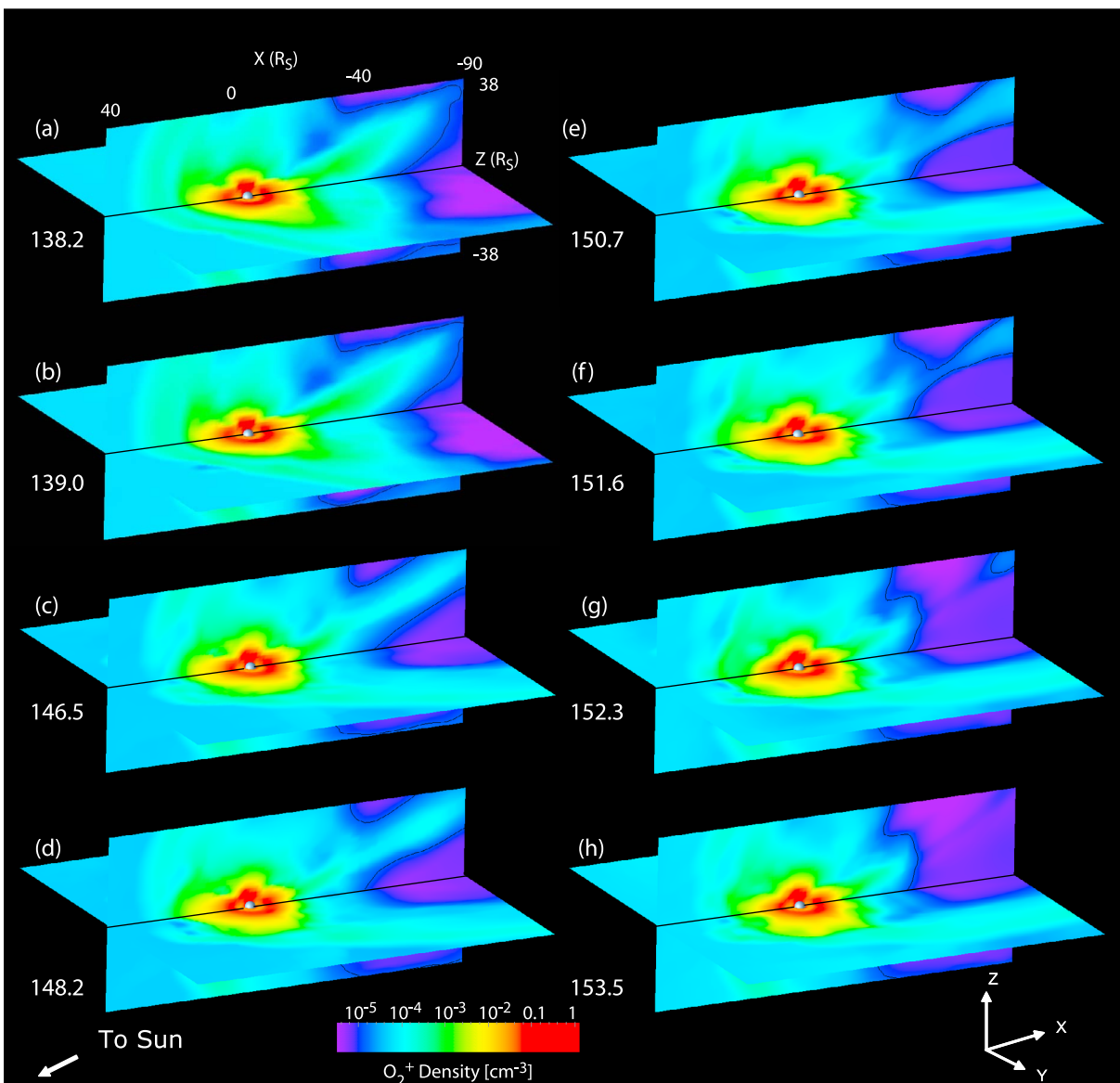


Figure 3. O_2^+ density in the equatorial and noon-midnight meridian planes. The direction of the sun is to the lower left. Inner magnetospheric plasma fills the plasma sheet, followed by thinning and reconnection. After the plasmoid exits the upper right corner of the slabs, plasma returns and moves Saturnward.

The plasmoid moves downtail with a speed of ~ 250 km/s. After reconnection, as the field lines (shown in Figure 2) become more dipolar, heavy plasma travels planetward.

[25] Looking at the magnetic field structure of plasmoids produced by one type of external triggering (a flip in the orientation of the IMF), Figure 4a shows a plasmoid that extends across the entire width of the tail. The white lines are the magnetic field lines and the O_2^+ density color contours show the density in the plane with the Enceladus torus. Its dimensions are $\sim 20 R_S$ in the x -direction and $\sim 53 R_S$ in the y -direction. In this frame the plasma sheet is tilted up and the plasmoid is currently $\sim 19 R_S$ above the equatorial plane. As the Kronian magnetosphere is affected by the change in the upstream conditions, the plasma sheet was $\sim 4 R_S$ thick and a bulge formed $\sim 40 R_S$ downtail. Plasma from the lobes filled the plasma sheet as it continued to grow in length. Reconnection occurred far from the planet at $\sim 60 R_S$. The

plasmoid travels downtail to the snapshot we see in Figure 4a, as it extends over both the pre- and post-midnight sectors. While Cassini has seen a number of plasmoids between 00 and 06 SLT due to the nature of its orbits, 3D modeling demonstrates that owing to the size of the plasmoid in the y -direction, there is no real local time or longitude to assign. Many plasmoids (such as seen in Figure 4a) may be much larger than the portion that sweeps over the Cassini spacecraft. This plasmoid is an example of the size and distance at which reconnection can occur for external triggering caused by a flip in the IMF. Complete development of the snapshot shown in Figure 4a is shown in Figure 5. With a view of the equatorial plane and O_2^+ density contours, the plasmoid may first be seen in the white magnetic field lines in Figure 5b before growing entirely across the tail in Figures 5c–5g and forming a horseshoe shape before moving

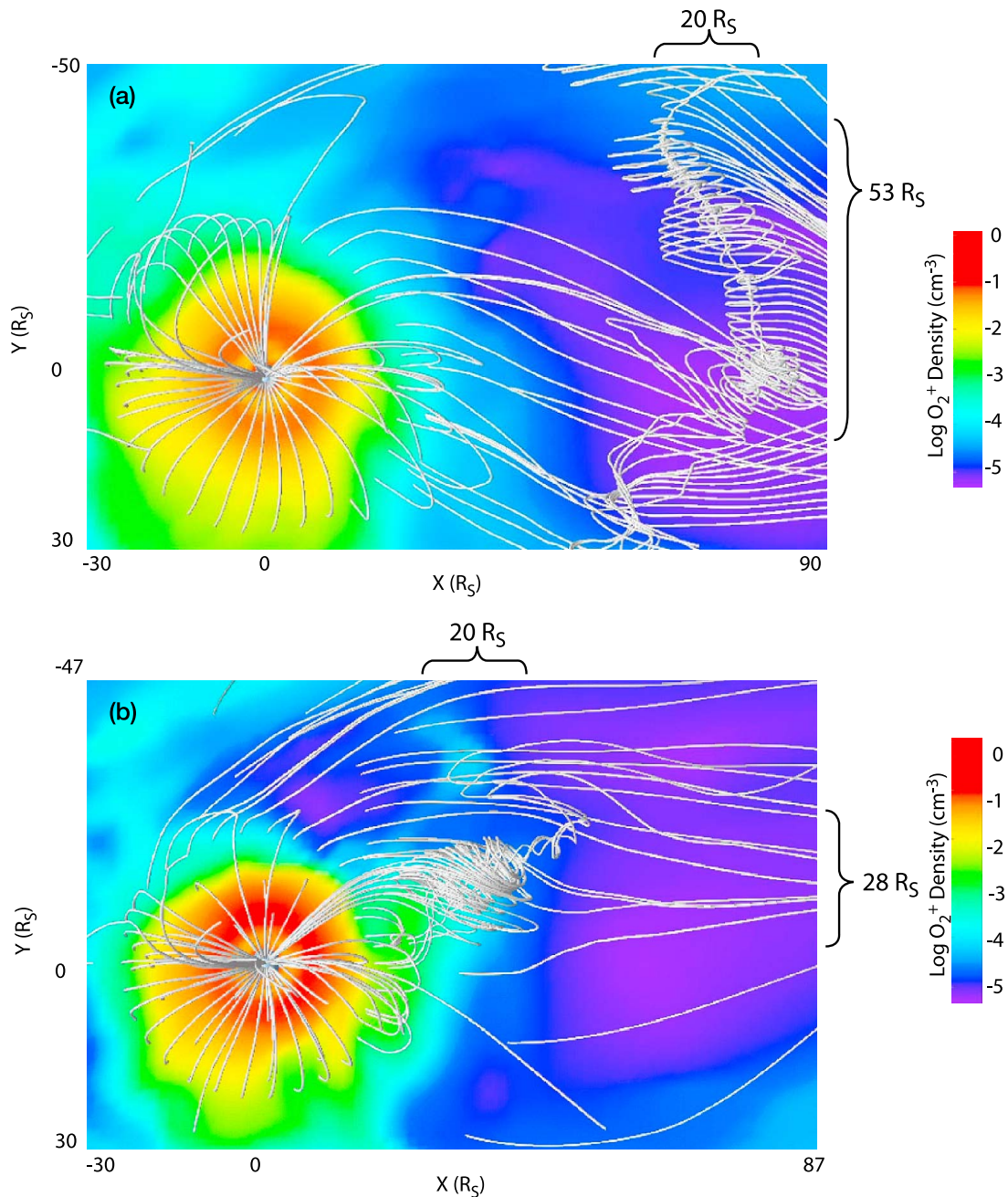


Figure 4. (a) Plasmoid triggered as a result of a flip in the IMF from parallel to antiparallel configuration. (b) Plasmoid triggered as a result of a pulsed increase in solar wind dynamic pressure. White magnetic field lines show the formation of plasmoids above the equatorial plane, O₂⁺ density contours in the equatorial plane below.

further downtail in Figure 5h. Again, this plasmoid occupies the entire crosstail region, and not one specific sector.

3.2. Triggering by a Pulse in the Solar Wind Dynamic Pressure

[26] Looking next at a plasmoid formed for external triggering as a result of a pressure pulse caused by a doubling of the solar wind dynamic pressure, Figure 4b shows a smaller plasmoid forming closer toward the planet. For these different solar wind conditions the plasma sheet is still tilted upward. The plasma sheet begins to thin, followed by the

formation of a structure analogous to a near Earth neutral line. Reconnection occurs at the neutral point closest to Saturn at $\sim 30 R_S$. This plasmoid actually started by the pre-midnight sector at a location of 22 SLT (for the center of the plasmoid structure). Saturn's rotation moves this plasmoid into the post-midnight sector where we can see in Figure 4b that it is more compact in the y -direction than the plasmoid shown in Figure 4a. It is $\sim 20 R_S$ in the x -direction, $\sim 28 R_S$ in the y -direction and $\sim 10 R_S$ above the equatorial plane in the z -direction. The development of the solar wind pressure triggered plasmoid can be seen in Figure 6. This plasmoid

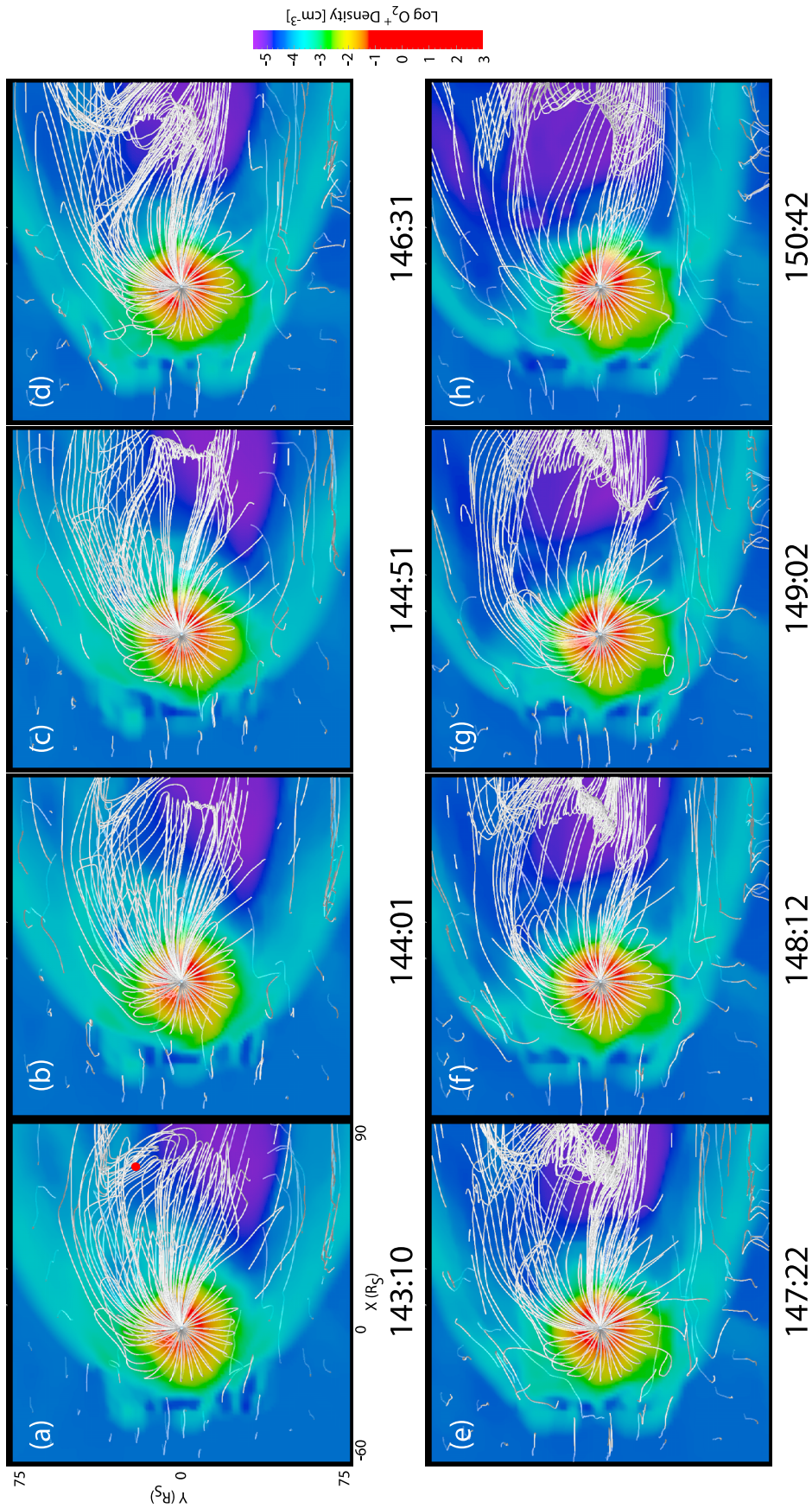


Figure 5. Development of a plasmoid triggered externally by a flip from parallel to anti-parallel IMF, as seen in Figure 4a, for a longer time period. Formation begins across the tail and expands into a horseshoe shape before moving downtail. O_2^+ density contours show the equatorial plane, but the white magnetic field lines are significantly above the crosstail current sheet at $\sim 20 R_S$.

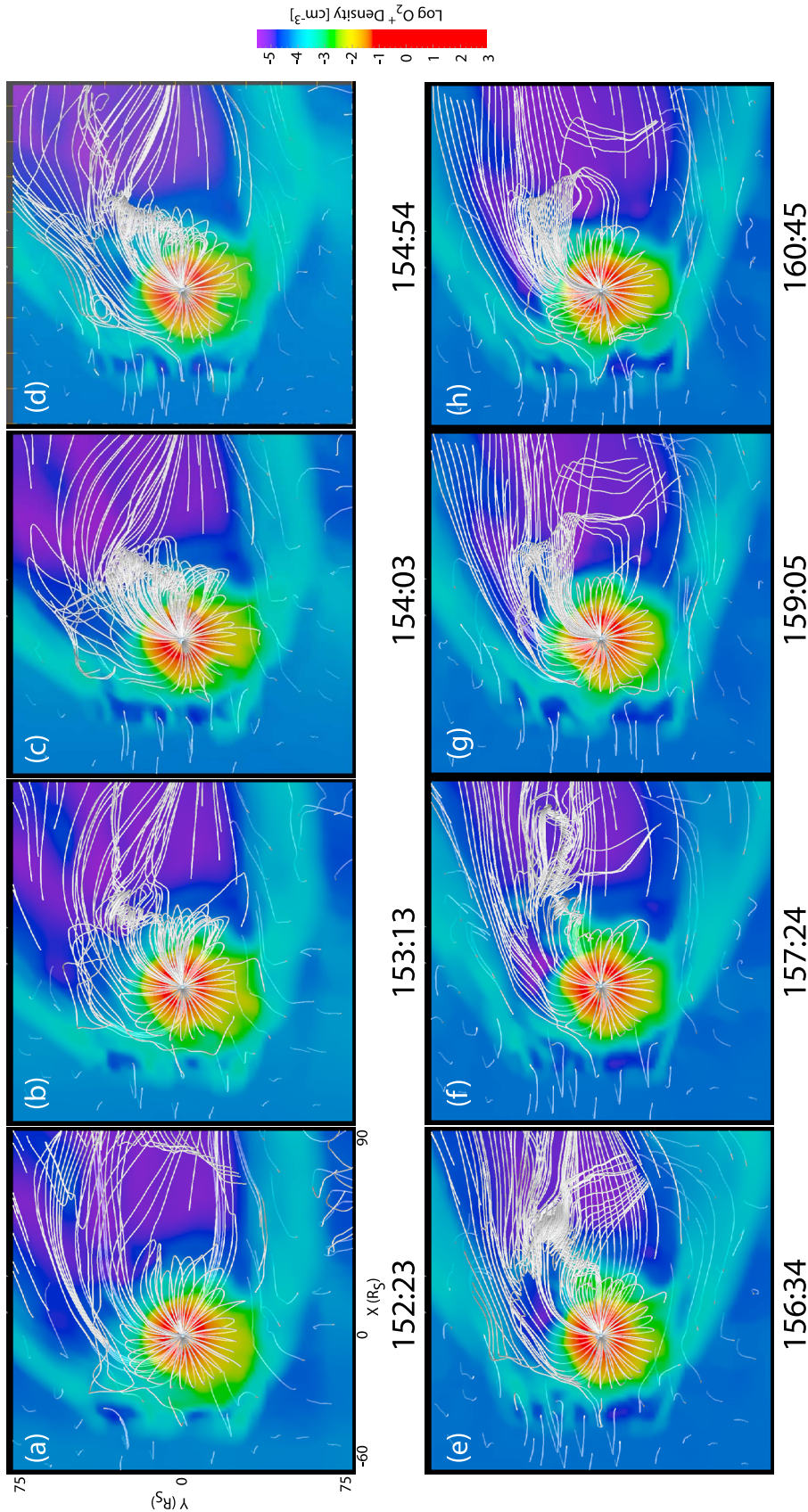


Figure 6. Same view of the O_2^+ density contours for the equatorial plane and white magnetic field lines, but for a plasmoid externally triggered by a pulse in the solar wind dynamic pressure, as seen in Figure 4b, but for a longer time period. This plasmoid forms much closer into the planet and as such is rotated into the post-midnight sector.

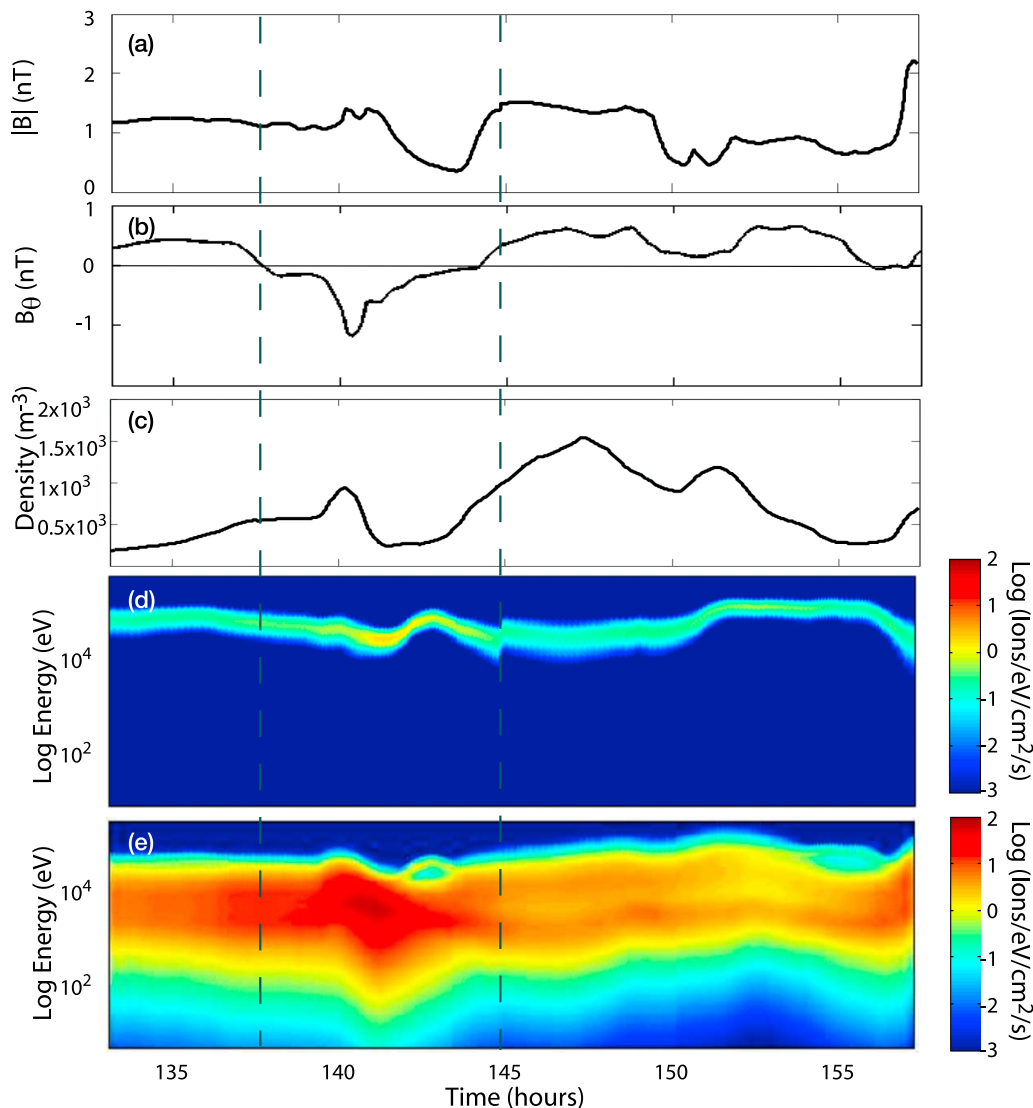


Figure 7. Magnetic and plasma signatures from a stationary synthetic spacecraft at $[80, 20, 30] R_S$ as a plasmoid washed over it: (a) magnetic field magnitude, (b) theta component of the magnetic field, (c) W^+ density, (d) O_2^+ spectrogram and all ions (H^+ , W^+ and O_2^+) spectrogram over time. Dashed lines denote the beginning and end of a plasmoid passing over the synthetic spacecraft. The antiparallel-IMF triggered plasmoid grazes the satellite at 141 h, and the pressure triggered plasmoid travels directly over the synthetic spacecraft at 153 h.

forms in the post-midnight sector (Figure 6b) but grows and twists in the x -direction as it moves up out of the equatorial plane (Figures 6c–6f).

[27] These two triggering conditions demonstrate that a flip in the configuration of the IMF produces a large plasmoid that covers most of the width of the tail, while a solar wind pressure pulse creates a more compact plasmoid closer in to the planet. Additionally, 3D modeling demonstrates that while the plasmoid in Figure 4b initially developed in the pre-midnight sector, rotation swept it into the dawn sector, so Cassini may be detecting plasmoid that formed in an area of the xy -plane different from where it was detected. In the primary part of its mission, Cassini was mainly in the equatorial plane and plasmoids were detected when the spacecraft made a plasma sheet crossing. 3D modeling allows us to see the truly three-dimensional nature of the plasmoids that travel

down the length of the plasma sheet as it is up out of the equatorial plane. It is important to note that plasmoids do not appear to form with every rotational period (i.e., approximately every 10.5 h). Our model demonstrates that plasmoids are not ejected periodically every 10.5 h. Instead, it may take 2.5–3 days, depending on upstream conditions, for a new plasmoid to form.

3.3. Magnetic Signatures and Plasmoid Composition

[28] The one-dimensional nature of Cassini MAG traces make it difficult to obtain three dimensional sizes and descriptions of the shapes of plasmoids in Saturn's magnetosphere. After using the multifluid model to characterize these plasmoid properties, we can compare the magnetic and plasma signatures indicative of the plasmoids with those observed by *Jackman et al.* [2007, 2008] in their papers. We

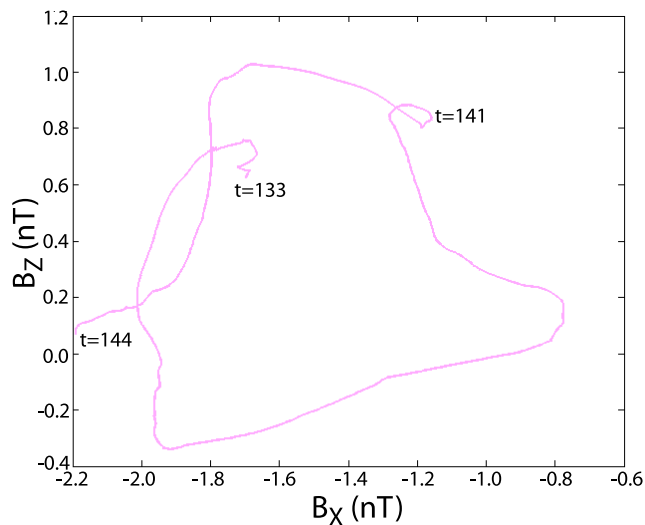


Figure 8. B_z versus B_x hodogram, based off measurements from the synthetic stationary spacecraft in Figure 7 for the times 133–144 h. Beginning at 133 h, time increases counterclockwise up to 144 h. The relatively circular shape indicates a plasmoid structure with current along the y axis.

placed synthetic spacecraft in the multifluid model directly in the path of a plasmoid forming and traveling downtail. This synthetic spacecraft give us magnetic field data (B_r , B_θ , B_ϕ , $|B|$) as well as electron and ion spectrogram data. The densities and speeds of each specific ion population can be plotted, since the multifluid model has four fluids with separate masses, velocities and temperatures.

[29] Figure 7 plots magnetic field, density and ion spectrogram data. This synthetic spacecraft was positioned at $[80, 20, 30] R_S$ (note the high latitude) while the plasmoids in Figures 5 and 6 washed over it. We can see how this matches the northward/southward magnetic signature that is characteristic of a plasmoid sweeping over the Cassini spacecraft. The large anti-parallel IMF triggered plasmoid grazes the synthetic satellite at 141 h, as evidenced by the fact that the B_θ component comprises the majority of $|B|$, making it nearly the magnitude of the total field. The B_θ component is northward turning, transitioning southward from >0 to quickly southward near 141 h and back again (Figure 7b). At this same time the density of the W^+ population increases (Figure 7c), as well as the O_2^+ ions (not pictured). The flux in all of the ions (Figure 7e) doubles. The plasmoid then moves downtail as seen in Figures 5b–5g. The second, solar wind pressure triggered plasmoid (whose development can be seen in Figures 6b–6h) travels directly over the synthetic spacecraft at 153 h. The multifluid model has the ability to plot an ion spectrogram of a single ion species (O_2^+ in this case for Figure 7d). An enhancement in this Enceladus heavy ion population is seen. These spectrograms confirm that inner magnetospheric ions are trapped in the plasmoid, which is moving downtail.

[30] Figure 7 demonstrates that plasmoids developing in the Saturn multifluid model have the same characteristics of the five plasmoids that were detected by Cassini. To aid in this visualization Figure 8 plots magnetic field data for the same synthetic spacecraft which generated the data in Figure 7 as a hodogram. As the axis of the first plasmoid is

primarily aligned along the y axis, the B_x and B_z components are plotted. A strong circular pattern shows that the plasmoid is complete in a manner associated with flux ropes and plasmoids [Cloutier *et al.*, 1999], definitively showing that the spacecraft has observed a plasmoid structure.

[31] Figure 9 gives us a sense of the composition inside a plasmoid. Each of the three ion populations (H^+ , W^+ and O_2^+) are shown in Figure 9 in the equatorial plane and a crosstail plane positioned at $x = 50 R_S$. Saturn is the small gray sphere and in each of these plots, the direction of the sun is to the lower left. The plasmoid traveling downtail can be more obviously seen in the crosstail W^+ cut. The kinked current sheet, clearly up out of the equatorial plane is fatter in the post-midnight section; this is the center of the plasmoid as it encounters this plane. The region of enhancement density is most keenly seen in the heavy ion populations, a similar enhancement is not seen in the lighter H^+ population. We can see from Figure 3 that the Enceladus plasma has been trapped during the plasmoid’s formation deep in the inner magnetosphere. W^+ densities are similar to those observed by Hill *et al.* [2008] (an increase from 10^{-3} to 10^{-2} for water group ions). The flux of W^+ and O_2^+ ions past the crosstail cut represent a lower limit for ions/s flowing past the y - z -plane at $50 R_S$ and show a slight increase during the plasmoid encounter for W^+ and an order of magnitude increase for O_2^+ ion (Figure 9). There is a semi-permanent feature of heavy ions moving down the low latitude boundary layer/magnetosheath due to the interaction of the interchange fingers with this boundary region and the enhanced densities in the mid-tail region are one effect of plasmoid ejection.

[32] Although the nightside current sheet flaps up and down relative to the equatorial plane, a global model allows us to characterize its hinging location and tilt angle, as well as the plasma sheet’s location relative to plasmoids. Cassini toured Saturn’s tail in 2006, sampling areas between 30 and $60 R_S$ downtail, primarily in the equatorial plane and primarily in the post-midnight sector. Infrequent plasma sheet crossings implied that the plasma sheet was frequently bent upward above Cassini’s orbits. Since the spacecraft spent a large portion of its time below the plasma sheet, it was likely located well below plasmoids that were forming and moving downtail. In the multifluid model, the plasma sheet is tilted upward approximately 10° from the equatorial plane and the hinging location is about $20 R_S$ downtail. The nightside thickness, in the absence of plasmoids, is generally $4 R_S$ thick. A day-night asymmetry is apparent in terms of plasma sheet thickness, with the dayside plasma sheet compressed by the magnetopause and forming a wedge from $\pm 70^\circ$ latitude. These plasma sheet observations are in agreement with Sergis *et al.* [2009] and the plasma sheet is indeed warped at all local times leading to its bowl-like morphology. The geometry of the plasma sheet changes and reacts to the upstream conditions. The plasma sheet is hinged upward prior to plasmoid formation. After a plasmoid exits the simulation the plasma sheet remains bent upwards for at least 10 h.

4. Conclusion

[33] This multifluid treatment of the Kronian magnetosphere provides information about the sizes and shapes of plasmoids in Saturn’s magnetotail as well locations in

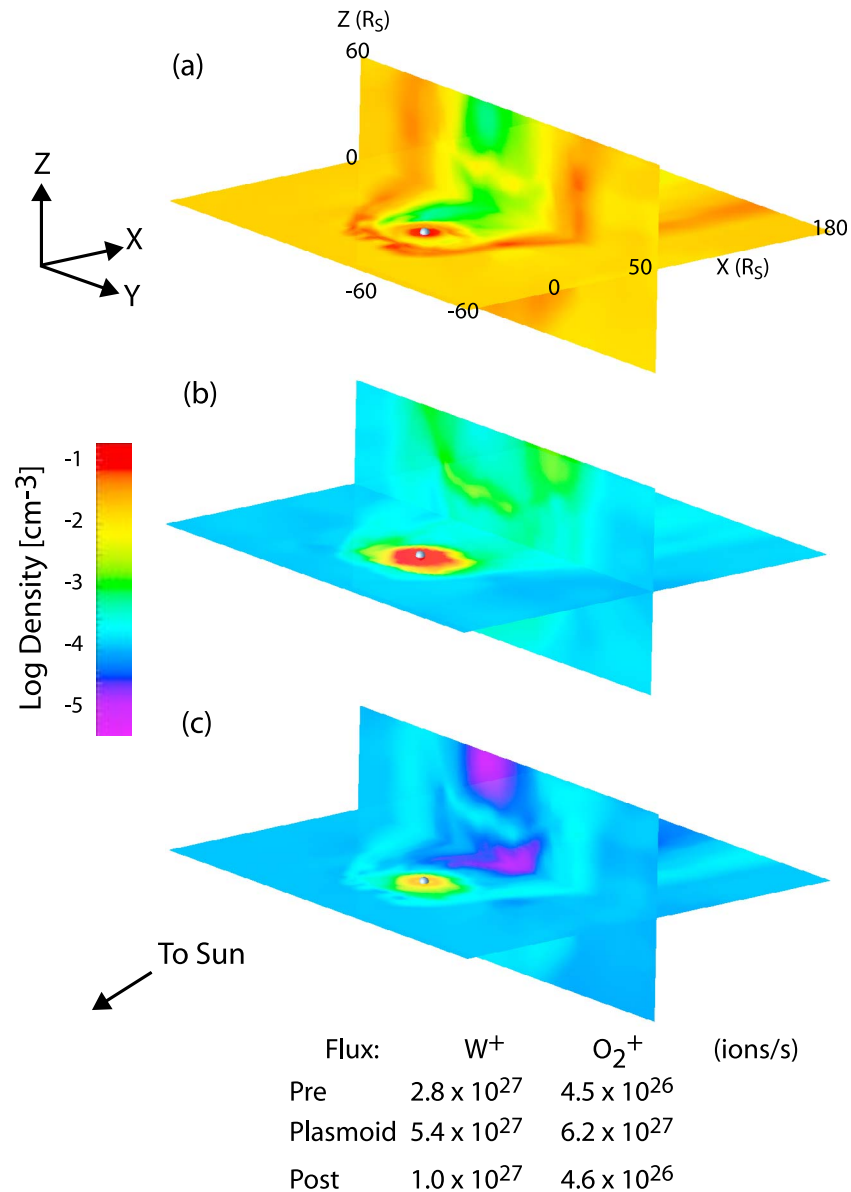


Figure 9. Ion composition of the plasmoid is dominated by heavy inner magnetospheric ions. Slabs with densities of the three different ion species: (a) H⁺, (b) W⁺ and (c) O₂⁺ in the equatorial and YZ crosstail planes. The crosstail plane is located 50 R_S downtail. The direction of the sun is toward the lower left of the figure. Fluxes for the heavy ions before, during and after the plasmoid passes by show an increase in W⁺ flux and an order of magnitude increase in O₂⁺ flux.

all three dimensions. The global nature of the multifluid model allows the spatial structure of both the individual plasmoid events and the global plasma sheet geometry to be characterized.

[34] While Cassini has observed plasmoid events which are believed to be produced by substorm-like events, its one-dimensional traces make it difficult to get a scope of the size and shape of a plasmoid. Additionally, orbital limitations hamper the ability to get a complete idea as to the formation locations and frequency of occurrence, and lack of ion moments makes composition measurements difficult.

[35] The multifluid model demonstrates that both flips in the orientation of the IMF as well as a pulse in the solar wind dynamic pressure can externally trigger plasmoids. The flip

in the IMF produced a large plasmoid >50 R_S which covered most of the width of the tail. The solar wind pressure pulse produced a smaller plasmoid ~28 R_S in size, closer in to the planet in the pre-midnight sector which subsequently rotated into the dawn sector. Both plasmoids are dominated by heavy ions and move downtail with speeds of ~250 km/s. The plasma sheet hinges ~20 R_S downtail and solar wind-forcing bends the plasma sheet up into a bowl shape at all latitudes at an angle of ~10°. While this work demonstrates that there are external triggers for plasmoid formation, the question of internal triggers for plasmoid formation at Saturn has yet to be answered. Future work will focus on determining the reconnection periodicity and its relation to rotation in the inner magnetosphere out to Titan's orbit at 20 R_S.

[36] **Acknowledgments.** Computer simulations run on the Atlas supercomputer at Georgia Tech. This grant was supported by NASA grant NNX07AJ80G to the University of Washington. This work was discussed in part at the International Space Science Institute with team number 195, “Dynamics of Planetary Magnetotails.”

[37] Masaki Fujimoto thanks the reviewers for their assistance in evaluating this paper.

References

- Arridge, C. S., K. K. Khurana, C. T. Russell, D. J. Southwood, N. Achilleos, M. K. Dougherty, A. J. Coates, and H. K. Leinweber (2008), Warping of Saturn’s magnetospheric and magnetotail current sheets, *J. Geophys. Res.*, *113*, A08217, doi:10.1029/2007JA012963.
- Brandt, P. C., K. K. Khurana, D. G. Mitchell, N. Sergis, K. Dialynas, J. F. Carbary, E. C. Roelof, C. P. Paranicas, S. M. Krimigis, and B. H. Mauk (2010), Saturn’s periodic magnetic field perturbations caused by a rotating partial ring current, *Geophys. Res. Lett.*, *37*, L22103, doi:10.1029/2010GL045285.
- Cloutier, P., et al. (1999), Venus-like interaction of the solar wind with Mars, *Geophys. Res. Lett.*, *26*, 2685–2688, doi:10.1029/1999GL900591.
- Crary, F. J., et al. (2005), Solar wind dynamic pressure and electric field as the main factors controlling Saturn’s aurorae, *Nature*, *433*, 720–722, doi:10.1038/nature03333.
- Fukazawa, K., S. Ogi, T. Ogino, and R. J. Walker (2007), Magnetospheric convection at Saturn as a function of IMF B_z , *Geophys. Res. Lett.*, *34*, L01105, doi:10.1029/2006GL028373.
- Hansen, K. C., A. J. Ridley, G. B. Hospodarsky, N. Achilleos, M. K. Dougherty, T. I. Gombosi, and G. Toth (2005), Global MHD simulations of Saturn’s magnetosphere at the time of Cassini approach, *Geophys. Res. Lett.*, *32*, L20S06, doi:10.1029/2005GL022835.
- Harnett, E. M., R. M. Winglee, and C. Paty (2006), Multi-scale/multi-fluid simulations of the post plasmoid current sheet in the terrestrial magnetosphere, *Geophys. Res. Lett.*, *33*, L21110, doi:10.1029/2006GL027376.
- Hill, T. W., et al. (2008), Plasmoids in Saturn’s magnetotail, *J. Geophys. Res.*, *113*, A01214, doi:10.1029/2007JA012626.
- Jackman, C. M., N. Achilleos, E. J. Bunce, S. W. H. Cowley, M. K. Dougherty, G. H. Jones, S. E. Milan, and E. J. Smith (2004), Interplanetary magnetic field at ~ 9 AU during the declining phase of the solar cycle and its implications for Saturn’s magnetospheric dynamics, *J. Geophys. Res.*, *109*, A11203, doi:10.1029/2004JA010614.
- Jackman, C. M., C. T. Russell, D. J. Southwood, C. S. Arridge, N. Achilleos, and M. K. Dougherty (2007), Strong rapid dipolarizations in Saturn’s magnetotail: In situ evidence of reconnection, *Geophys. Res. Lett.*, *34*, L11203, doi:10.1029/2007GL029764.
- Jackman, C. M., et al. (2008), A multi-instrument view of tail reconnection at Saturn, *J. Geophys. Res.*, *113*, A11213, doi:10.1029/2008JA013592.
- Jackman, C. M., L. Lamy, M. P. Freeman, P. Zarka, B. Cecconi, W. S. Kurth, W. H. Cowley, and M. K. Dougherty (2009), On the character and distribution of lower-frequency radio emissions at Saturn and their relationship to substorm-like events, *J. Geophys. Res.*, *114*, A08211, doi:10.1029/2008JA013997.
- Jackman, C. M., J. A. Slavin, and S. W. H. Cowley (2011), Cassini observations of plasmoid structure and dynamics: Implications for the role of magnetic reconnection in magnetospheric circulation at Saturn, *J. Geophys. Res.*, *116*, A10212, doi:10.1029/2011JA016682.
- Kidder, A., R. M. Winglee, and E. M. Harnett (2009), Regulation of the centrifugal interchange cycle in Saturn’s inner magnetosphere, *J. Geophys. Res.*, *114*, A02205, doi:10.1029/2008JA013100.
- Liu, X., T. W. Hill, R. A. Wollf, S. Sazykin, R. W. Spiro, and H. Wu (2010), Numerical simulation of plasma transport in Saturn’s inner magnetosphere using the Rice Convection Model, *J. Geophys. Res.*, *115*, A12254, doi:10.1029/2010JA015859.
- Paty, C., J. Dufek, J. H. Waite, and R. L. Tokar (2011), Coupling eruptive dynamics models to multi-fluid plasma dynamic simulations at Enceladus, Abstract SM21B-2017 presented at 2011 Fall Meeting, AGU, San Francisco, Calif., 5–10 Dec.
- Sergeev, V., et al. (2003), Current sheet flapping motion and structure observed by Cluster, *Geophys. Res. Lett.*, *30*(6), 1327, doi:10.1029/2002GL016500.
- Sergis, N., S. M. Krimigis, D. G. Mitchell, D. C. Hamilton, N. Krupp, B. H. Mauk, E. C. Roelof, and M. K. Dougherty (2009), Energetic particle pressure in Saturn’s magnetosphere measured with the Magnetospheric Imaging Instrument on Cassini, *J. Geophys. Res.*, *114*, A02214, doi:10.1029/2008JA013774.
- Snowden, D., R. Winglee, C. Bertucci, and M. Dougherty (2007), Three-dimensional multifluid simulation of the plasma interaction at Titan, *J. Geophys. Res.*, *112*, A12221, doi:10.1029/2007JA012393.
- Snowden, D., R. Winglee, and A. Kidder (2011a), Titan at the edge: 1. Titan’s interaction with Saturn’s magnetosphere in the prenoon sector, *J. Geophys. Res.*, *116*, A08229, doi:10.1029/2011JA016435.
- Snowden, D., R. Winglee, and A. Kidder (2011b), Titan at the edge: 2. A global simulation of Titan exiting and reentering Saturn’s magnetosphere at 13.6 Saturn local time, *J. Geophys. Res.*, *116*, A08230, doi:10.1029/2011JA016436.
- Winglee, R. M. (2004), Ion cyclotron and heavy ion effects on reconnection in a global magnetotail, *J. Geophys. Res.*, *109*, A09206, doi:10.1029/2004JA010385.
- Winglee, R. M., E. Harnett, and A. Kidder (2009), Relative timing of substorm processes as derived from multifluid/multiscale simulations: Internally driven substorms, *J. Geophys. Res.*, *114*, A09213, doi:10.1029/2008JA013750.
- Young, D. T., et al. (2005), Composition and dynamics of plasma in Saturn’s magnetosphere, *Science*, *307*, 1262–1266, doi:10.1126/science.1106151.
- Zieger, B., K. C. Hansen, T. I. Gombosi, and D. L. DeZeeuw (2010), Periodic plasma escape from the mass-loaded Kronian magnetosphere, *J. Geophys. Res.*, *115*, A08208, doi:10.1029/2009JA014951.